

Theoretical and Raman Spectroscopic Studies of Phenolic Lignin Model Monomers

Kiki L. Larsen[†] and Søren Barsberg*

Faculty of Life Sciences, University of Copenhagen, Rolighedsvej 23, DK - 1958 Frederiksberg C, Denmark

Received: March 29, 2010; Revised Manuscript Received: May 4, 2010

Structural analysis of plant materials supports the growing interest in their use for chemicals, for example, biofuels. Lignin is a main polymer component formed from three phenolic precursors containing none, one or two OMe groups, i.e. H, G and S units, respectively. Raman spectroscopy offers structural information on lignin. This relies on correct assignment of observations to fundamental vibrations, and today this subject is not without controversy. The present work shows the strength of *first principles* assignment of lignin model bands. Raman spectra of three H, G, and S phenolic end group models are compared with density functional theory predictions of their vibrational properties. H, G, and S marker bands are found and related to specific vibrations. For the S unit, multiple OMe conformations exist that may all contribute to its Raman spectrum. Two ring deformation modes at $\sim 1600\text{ cm}^{-1}$ offer a potential route of gaining information on the microenvironment.

Introduction

Lignin is together with cellulose and hemicelluloses an integral part of plant cell walls, for example, wood cells, and is one of the most abundant plant polymers on earth.¹ The exact structure of lignin is not well-defined, but in terms of linkage types, substitution patterns, and so on, it varies between plant species, between cell types within a single plant, and between different parts of the wall of a single cell.² Its basic chemical structure and modifications can be detected by vibrational spectroscopy.^{3–5}

For vibrational spectroscopy, the assignment of lignin bands provides the crucial link between experimental data and structural knowledge. A classic approach has relied on qualitative analogues of lignin substructures, such as carbonyl groups, phenols, methoxy groups, aromatic rings, ether linkages, and so on, to other simpler compounds containing these. This has given rise to “spectroscopic charts” relating substructural elements to their typical vibrational properties.

Raman spectroscopy is in particular a useful vibrational spectroscopic tool in the investigations of the chemical components of wood and plant materials, and especially lignin, because no sample preparation is needed. Laser-induced auto fluorescence from lignin can be the major hindrance to obtaining reasonably good Raman spectra because the fluorescence intensity can be several orders of magnitude larger than the Raman scattering intensity. Traditionally, two sampling procedures were used to effectively reduce the auto fluorescence: water immersion technique (usable for woody tissues)⁴ and oxygen flushing technique.^{3,6} Fluorescence problems can be reduced by choosing the near-IR Fourier transform Raman technique (NIR-FT), using a NIR laser source with a photon energy well below troublesome low energy electronic transitions of lignin. By applying this method, good quality spectra, relatively free of fluorescence interference, from various lignin-containing materials were obtained.^{7–11} Today, also more sophisticated spectroscopic methods can overcome this problem.

UV resonance Raman spectroscopy exploits the combined benefit of the resonantly enhanced Raman signal and the usually relatively much longer wavelengths of fluorescence emission compared to Raman photons. Kerr gated Raman spectroscopy^{12–15} exploits the different time-domain characteristics of fluorescence and Raman emission by allowing the detector only to see a narrow time-domain window centered on the excitation laser pulse.^{16–18} Whereas Raman spectroscopy of lignin-containing samples thus has experienced significant developments this has not been paralleled from a theoretical side.

The advent of density functional theory (DFT),^{19,20} and its immense practical gain of strength seen from the 1990s and onward, has enabled a more reliable prediction of vibrational bands and not the least their associated intensities, which is not based on empirical data (apart from the parametrization of functionals), but on first principles, that is, basic electronic structure theory. The introduction of the B3LYP density functional^{21–24} has played a decisive role in this respect and it is known to perform well for vibrational properties.

Some of the most important and reactive lignin moieties are the phenolic end groups, which are susceptible to oxidation (they have a relatively low redox potential) and thus play important roles in lignin biosynthesis and biodegradation. In the present work we focus on three finite sized models of such moieties, which carry the three possible distinguishing lignin methoxy group substitutions, that is, *p*-hydroxyphenyl (H: 4-methylphenol), guaiacyl (G: 2-methoxy-4-methylphenol), and syringyl (S: 2,6-dimethoxy-4-methylphenol) moieties. For the sake of computational feasibility the methyl group substitutes for the (continued) lignin polymer.

The three models, which will also be referred to in the following as H-unit, G-unit, and S-unit, are displayed in Figure 1. The numbering applied starts the carbon numbering from the phenolic carbon (1) and counting clockwise. For carbon and oxygen atoms, they are numbered as C1–C7, O1 (H unit), C1–C8, O1, O2 (G-unit), and C1–C9, O1–O3 (S unit). The hydrogen atoms are numbered according to the atom to which they are attached, for example, O1–H1, C7–H7a, C7–H7b, and so on. This has been done to ease the comparison between the models, because all C and O atoms have the same numbers

* To whom correspondence should be addressed: Phone: +45 35331686. Fax: +45 35331508. E-mail: sbar@life.ku.dk.

[†] Present address: Technical University of Denmark, Institute of Environmental Engineering, Miljøvej, DK-2800 Kgs Lyngby, Denmark.

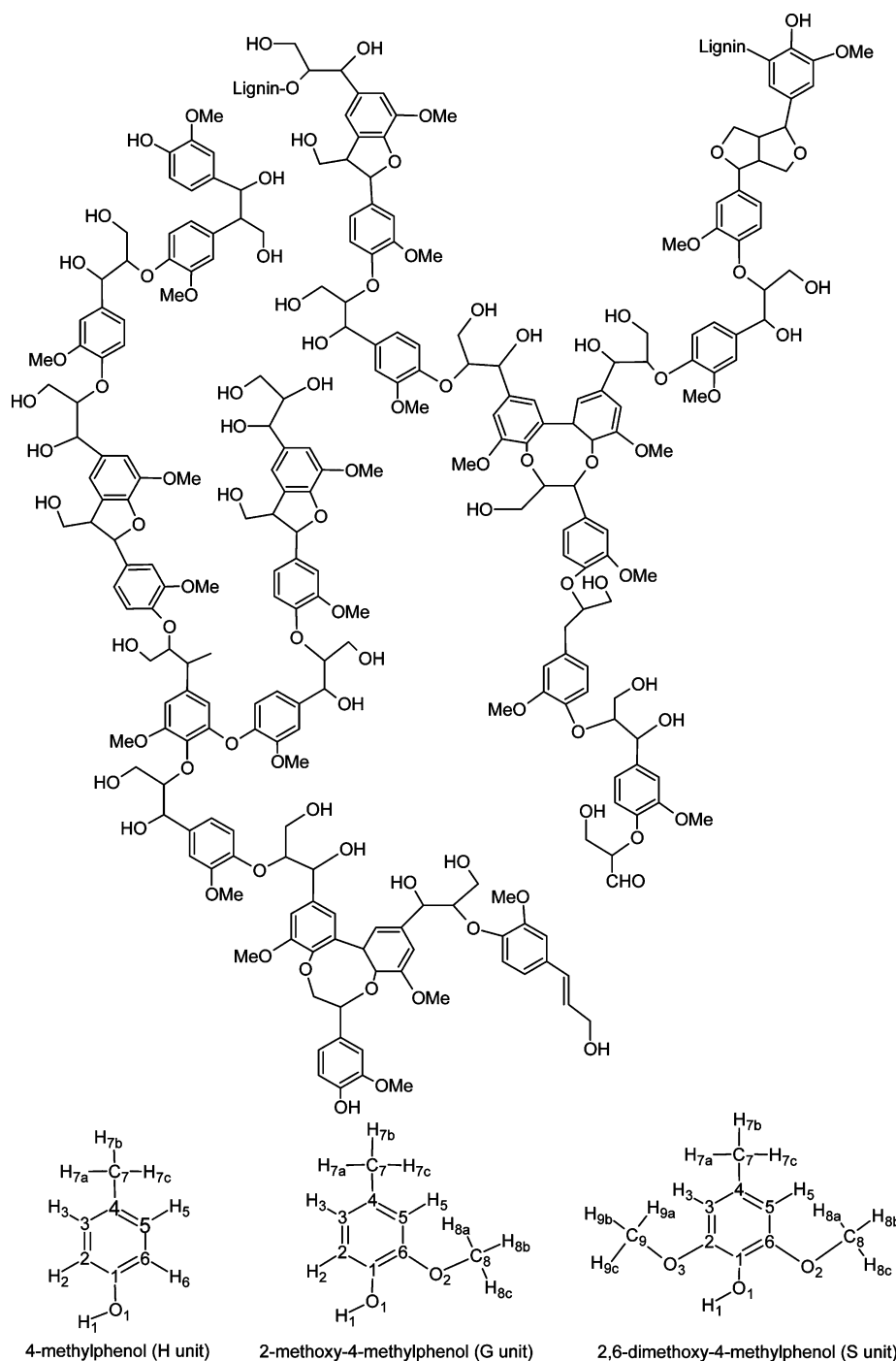


Figure 1. Tentative lignin structure reproduced from ref 25 and the three phenolic lignin model monomers.

in the different models. The lignin structure has been reproduced from reference.²⁵

The DFT based modeling of lignin vibrational properties must necessarily make some practical assumptions. Because lignin consists of aromatic structures, linked via C–O and *saturated* C–C linkages, its high frequency vibrations are to a good approximation localized to these. A refinement of this description, which we do not consider here, would consider vibrational coupling between these structures. Though the errors imposed by simple isolated structure models of lignin are not large, the *practice* of assigning vibrational bands to structural moieties suggests the same.

To obtain a basic understanding of the vibrational properties, it is important that these refer to weak or no interactions with

the environment. In the present work, this is achieved by obtaining Raman spectra from the model compounds dissolved in CCl₄, which is a weakly interacting nonpolar solvent, and subjecting the model structures to B3LYP calculations of vibrational properties in simulated CCl₄ environment. The solvent effect was modeled by the Polarizable Continuum Model (PCM) as invented by Tomasi and co-workers and implemented in the Gaussian software package.²⁶ The strength and necessity of DFT-based predictions is exemplified, as will be shown, by the predicted *triple potential energy well* of the non-H-bonded OMe group of the S-unit structure. These multiple minima must all be accounted for if one wishes an appropriate prediction and description of the Raman spectrum of such a lignin substructure and hence of lignin.

The general goal of our research of lignin models is thus through electronic structure calculations to enable the achievement of spectroscopic information that can help gain a better understanding of the structure and processes of lignin containing materials, for example, understanding lignin polymerization or degradation processes.

Experimental Methods

Chemicals. 4-Methylphenol (99%, *p*-cresol), 2-methoxy-4-methylphenol (99%, *p*-creosol), 2,6-dimethoxy-4-methylphenol (97%), and CCl₄ were obtained from Sigma-Aldrich and used as received.

Samples. *p*-Cresol (*l*), *p*-creosol (*l*), or 2,6-dimethoxy-4-methylphenol (*s*) was mixed/dissolved in CCl₄, each in different w/w% ratios ranging from 2–80%, and were transferred to small glass tubes, 2 mm in diameter, which were sealed and used in the Raman spectrometer.

Raman Spectroscopy. The Raman spectra were obtained using a Bruker RFS 100 FT-Raman spectrometer. The laser used was a Nd:YAG laser at 1064 nm with intensity 280 mW and a spectral resolution of 4 cm⁻¹. The interferogram was zero-filled*2 and a Blackmann-Harris apodization function was used giving an effective spectral resolution of 6 cm⁻¹. The wavenumbers were calibrated using the characteristic band positions from cyclohexane,²⁷ which is a recommended frequency standard.²⁸

Spectral Manipulation. The spectra were corrected by subtracting the CCl₄ contribution. The intense CCl₄ band at approximately 460 cm⁻¹ was used to scale the CCl₄ spectrum for subtraction. Curve fitting was performed with the program Microcal ORIGIN, version 8. Bands were fitted using superimposed Lorentzian or Gaussian band shapes, and it was found that Lorentzian band shapes gave the best fit. Thus, Lorentzian band shapes were assumed, and the observed band frequencies refer to the center position of these bands.

Modeling of Vibrational Properties. Harmonic frequencies, Raman intensities, and anharmonic frequency shifts (in CCl₄) of the model compounds were predicted using the G03 software package.²⁶ Vibrations were visualized by the Gausview software. For harmonic frequencies and Raman intensities the B3LYP functional was used with the 6-31+G(d) basis set, and “tight” geometry convergence (<10⁻⁶ au root mean square (rms) force, <4 × 10⁻⁶ au rms displacement), “tight” self-consistent field (SCF) convergence (<10⁻⁸ au rms density matrix), and the “ultrafine” integration grid (i.e., 99 radial shells and 590 angular points) if nothing else is stated. The CCl₄ solvent effects were predicted by the PCM using the United Atoms Hartree–Fock (UAHF) radii and default settings. All optimized structures represent true energy minima as no imaginary frequencies were produced. A factor *f* = 0.9636 corresponding to the chosen basis set was used for scaling all harmonic frequencies.²⁹

Anharmonic frequency shifts $-\omega_{\text{AH}}$ were derived from an HF/6-31G(d) anharmonic frequency calculation, which was combined with the same PCM model of the solvent. The shifts were obtained from a single calculation as the difference between harmonic and anharmonic frequencies (neglecting any additional calculated perturbative shift, for example, Fermi resonance). The desired anharmonic frequency $\omega_{\text{PCM}} - \omega_{\text{AH}}$ was then approximated by the sum of the (nonscaled) B3LYP/6-31+G(d) harmonic frequency ω_{PCM} and HF/6-31G(d) anharmonic shift $-\omega_{\text{AH}}$.

For 2,6-dimethoxy-4-methylphenol, the population probabilities of the methoxy conformers were estimated based on their relative free energies. These were derived from first a refinement of the (vacuum) geometries using B3LYP/cc-pVTZ

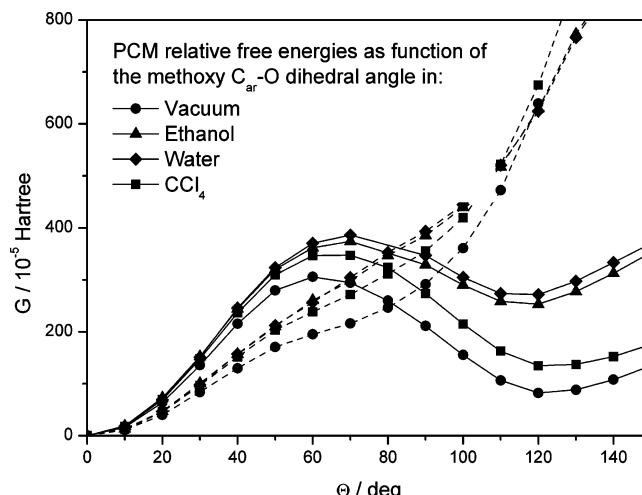


Figure 2. PCM relative free energies as function of the methoxy C_{ar}–O dihedral angle: dotted lines, the hydrogen bonded methoxy group; straight lines, the nonhydrogen bonded methoxy group.

optimization and subsequent MP2 single point energies using the aug-cc-pVXZ (X = D and T) basis sets extrapolated to the complete basis set (CBS) limit $E_{\text{MP2,CBS}}$ and, second, the B3LYP/6-31+G(d)/PCM (CCl₄) solvation free energies $\Delta g(\text{vac} \rightarrow \text{CCl}_4)$ derived from a vacuum and a PCM geometry optimization and frequency calculation using the same settings as above. For each conformer *i*, the free energy G_i in CCl₄ solvent is then $G_i = E_{\text{MP2,CBS}} + g_{\text{vib}}(\text{vac}) + \Delta g(\text{vac} \rightarrow \text{CCl}_4)$, where $g_{\text{vib}}(\text{vac})$ is the vibrational free energy component in vacuum (vac). Conformer probabilities p_i are then given by $p_i = A \exp(-G_i/k_B T)$, where *A* is determined by the normalization condition $\sum p_i = 1$.

Results

Before considering the predicted and observed Raman spectra of the three lignin model monomers, it is important to realize that some of the models can adopt different conformations.

2-Methoxy-4-methylphenol. 2-Methoxy-4-methylphenol has four different conformers defined by the hydroxy and methoxy group orientations. The *transoid* structures differ by orientation of the methoxy group in and out of the aromatic plane. These are defined by four sets of the two dihedral angles, C6–C1–O1–H1 and C5–C6–O2–C8 (see Figure 1), which are respectively (cisoid) 0°, 0°; (transoid 1) −180°, 0°; (transoid 2) −180°, 112°; and (transoid 3) 180°, −112°. Transoids 2 and 3 are mirror images and equal in energy. Equivalent conformers have been investigated for guaiacol (2-methoxyphenol) by Agache and Popa.³⁰ They evaluated the higher stability of the cisoid conformer of guaiacol in relation to the transoid conformers to be in the range 18.09–18.51 kJ/mol based on second-order (MP2) and fourth-order (MP4SDQ) Møller–Plesset theory. This high stability of the lowest energy structure is due to the intramolecular hydrogen bond between the phenolic hydrogen and the free electron pair of the methoxy oxygen. On this background, only the cisoid structure was selected for modeling.

2,6-dimethoxy-4-methylphenol. For this compound only one of two methoxy groups can function as acceptor in intramolecular hydrogen bonding. The rotational flexibility around the C_{ar}–O bonds of the methoxy groups was examined using the PCM/B3LYP/6-31G(d) method. In Figure 2, eight free energy profiles are displayed. Four profiles show the hydrogen bonded methoxy group (dotted lines) and four profiles show the

TABLE 1: Probability Distribution at $T = 300$ K of the Two Different Conformations Calculated by B3LYP and MP2 Methods

conformation	$\Theta \approx 0^\circ$		$\Theta \approx 120^\circ*$	
calculation	G (Hartree)	$P\%$	G (Hartree)	$P\%$
B3LYP/6-31+G(d)	-575.6886270	47.3	-575.6880740	52.7
MP2/aug-cc-pVDZ	-574.2762076	55.3	-574.2753510	44.7
MP2/aug-cc-pVTZ	-574.7821783	72.6	-574.7806044	27.4
MP2/aug-cc-pV ∞ Z	-574.9952186	78.5	-574.9933426	21.5

* The 120° conformer contributes twice to the statistics.

nonhydrogen bonded methoxy group (straight lines), both in four different environments: vacuum, carbon tetrachloride, ethanol, and water.

It can be seen from the Figure 2 that only the methoxy group that does *not* act as hydrogen bonding acceptor has two minima. The second minimum is lower in energy in the non polar environment where a free energy of only $\sim 10^{-3}$ Hartree above that of the $\Theta = 0^\circ$ conformer is reached. As this energy is comparable to the thermal energy $k_B T$ ($T \sim 300$ K) *both* conformers must be included in the investigations, especially because the two conformations display different vibrational characteristics.

The conformation distribution calculated using B3LYP/6-31+G(d) displays an even distribution. Though, when evaluating the relative energies, an even better approach is to use Dunning type basis sets³¹ that, as opposed to the Pople^{32–35} type basis set, are designed to converge systematically to the complete basis set limit (CBL). Therefore, the energies of the two conformations have also been evaluated using the MP2 method and Dunning type basis sets, that is, MP2/aug-cc-pV ∞ Z (X = 2 and 3) energies calculated for the B3LYP/6-31+G(d) optimized structure. The two results were extrapolated to the CBL according to the expression $E_\infty = E_X + AX^{-3} + O(X^{-4})$ (see, e.g., Helgaker et al.³⁶), giving the MP2/aug-cc-pV ∞ Z result. In Table 1, the probabilities of the two conformations (counting the 120° conformer twice) are predicted in vacuum. The MP2/aug-cc-pV ∞ Z result is assumed to give the best estimated distribution of the two conformations, which is seen to contain a significant 22% fraction of the 120° conformer.

The PCM/B3LYP free energy profiles suggest that this conformer becomes less important as the polarity of the environment increases.

Comparing the Calculated and Experimentally Obtained Data. In Figure 3, the 1700 – 300 cm^{-1} interval of the experimental as well as the calculated Raman spectrum of the H-unit is displayed.

A good correlation between the calculated and the experimentally obtained spectrum is observed. Some discrepancies can be found, but none that prevents a fruitful comparison of experimental and calculated data. When two (or more) frequencies from the calculated H-unit vibrations coincide with one experimental band, both predicted bands are compared with the experimental band and guidance for the assignment is obtained from predicted versus observed intensities. This is the procedure for all three models.

Nomenclature when Comparing Experimental Raman Data with Calculated Raman Data. To shorten the descriptions the following notation is used. The in-plane and out-of-plane vibrations are abbreviated ip and oop, respectively, and refer always to the plane of the benzene ring, C_{ar} is a carbon atom in the benzene ring, O_(CH₃) is the oxygen(s) of the methoxy group(s), and O_(H) is the oxygen of the hydroxy group. CH₃

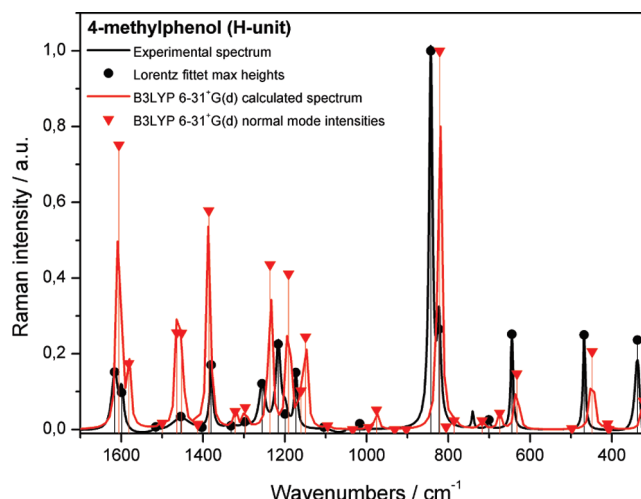


Figure 3. Interval of 1700 – 300 cm^{-1} of the Raman spectrum of 4-methylphenol: black line, experimental spectrum; black circles, heights of the Lorentz fitted bands; red line, calculated spectrum; red triangles, B3LYP/6-31+G(d) calculated Raman intensities in CCl₄. The calculated frequencies have been scaled by a factor of 0.9636.

and (O)CH₃ refer to the methyl group directly attached to the ring or as part of the methoxy group, respectively.

The vibrations are divided into three different categories: The C–H and O–H stretching region above 2500 cm^{-1} (str), the ip vibrations (below 2500 cm^{-1}), and the oop vibrations (below 2500 cm^{-1}).

Because for all models the fundamentals with a frequency less than 300 cm^{-1} were predicted to have <3.4 Raman activity (average: 0.6 $\text{\AA}^4/\text{amu}$) and as spectra could not be obtained below 300 cm^{-1} , these are neglected in this study.

The spectral changes when increasing the w/w% concentration of the model monomers were followed (results not shown), and no change in band positions or relative intensities were observed. Therefore, the highest possible concentration was used for deriving Raman band data, still allowing the compound to be soluble in carbon tetrachloride.

In Tables 2–4 the observed and predicted normal modes of the three models are displayed.

The Raman spectra have been divided into three main regions: >2500 cm^{-1} , 1700 – 1100 cm^{-1} , and <1100 cm^{-1} . Also, if not stated otherwise, when a calculated frequency from the S unit is given, it always refers to the 0° conformer. The assignment of all vibrations can be deduced from the tables, but to compare the differences and similarities of the three lignin model monomers they are also included and discussed in the text.

3150–2500 cm⁻¹. The OH stretching mode from all three compounds, predicted to lie in the interval 3500 – 3600 cm^{-1} , have not been observed due to instrumental cutoff at 3500 cm^{-1} .

In Figure 4, the interval from 3200 to 2600 cm^{-1} of the spectra of the three lignin model monomers is shown. Assigning the different vibrations to these bands is all but trivial due to the poor correspondence of observed and calculated frequencies even when scaling the calculated harmonic frequencies or taking anharmonic contribution into account. This can be a shortcoming of the B3LYP functional, but the limited quality basis set as well as resonance perturbations (e.g., Fermi resonances) in this part of the spectrum can also contribute.

A complete assignment of experimental bands is provided but is thus tentative.

3100–2980 cm⁻¹. The interval between 3100 and 2980 cm^{-1} displays three bands for the H and G unit and two bands for the S unit.

TABLE 2: Predicted and Observed Raman Data for 4-Methylphenol^a

Mode	Specific atoms involved in the vibration	Details	Type	ω_{PCM} scaled (cm ⁻¹)	$\omega_{\text{PCM}} - \omega_{\text{AH}}$ (cm ⁻¹)	Exp (cm ⁻¹)	I _{Raman} Exp	I _{Raman} PCM
Q42	v(O ₁ -H ₁)	ip OH str	str	3586	3547			173
Q41	v(C ₂ -H ₂)	ip CH str	str	3088	3080	3062	s	233
Q40	v(C ₅ -H ₅)	ip CH str	str	3067	3051			209
Q39	v(C ₃ -H ₃)	ip CH str	str	3057	3048	3039	m	127
Q38	v(C ₆ -H ₆)	ip CH str	str	3048	3038	3014	m	110
Q37	v(C ₇ -H _{7a})	oop str, Me	str	2999	3001			93
Q36	v _a (C ₇ -H _{7b} ; C ₇ -H _{7c})	oop asym str, Me	str	2971	2946	2922	s	131
Q35	v _s (C ₇ -H ₃)	oop sym str, Me	str	2925	2927	2867	m	320
Q34	v _s (C ₅ -C ₆ ; C ₂ -C ₃), δ (C _{ar} -H)	C _{ar} -C _{ar} sym str, C _{ar} -H bend dir1	ip	1606	1629	1616	s	40
Q33	v _s (C ₁ -C ₆ , C ₃ -C ₄), δ (C _{ar} -H), δ (OH)	C _{ar} -C _{ar} sym str, COH bend dir2	ip	1582	1603	1599	s	9.3
Q32	δ (C _{ar} -H), v(C _{ar} -C _{ar}), v(C-O)	C _{ar} -H ip bend and CO _(H) str and	ip	1500	1516	1516	w	0.9
Q31	γ (C ₇ -H ₃)	CH ₃ scissoring, Me	oop	1464	1479	1455	m	14
Q30	γ (C ₇ -H ₃)	CH ₃ scissoring, Me	oop	1453	1497			14
Q29	δ (OH), δ (C _{ar} -H), v _a (C ₂ -C ₃ ; C ₅ -C ₆)	rd and ip bend	ip	1413	1441	1403	w	0.8
Q28	γ _s (C ₇ -H ₃)	umbrella bend, Me	oop	1386	1456	1380	s	31
Q27	δ (OH), δ (C _{ar} -H), v(C _{ar} -C _{ar})	COH ip bend and rd	ip	1321	1344	1331	m	2.6
Q26	δ (C _{ar} -H), v(C _{ar} -C _{ar})	rd and ip bend	ip	1297	1321	1298	m	3.1
Q25	v(C ₁ -O ₁), δ (C _{ar} -H), v(C _{ar} -C _{ar})	C _{ar} -O str	ip	1236	1256	1256	s	23
Q24	v(C ₇ -C ₄), δ (C _{ar} -H), v(C _{ar} -C _{ar})	rd and C _{ar} -C str	ip	1191	1214	1216	s	22
Q23	δ _s (C _{ar} -H)	C _{ar} -H ip bend	ip	1160	1191	1199	m	5.5
Q22	δ (OH)	COH ip bend	ip	1149	1178	1173	s	13
Q21	δ (C _{ar} -H)	C _{ar} -H ip bend	ip	1095	1124	1105	w	0.6
Q20	γ (C ₄ -C ₇ -H)	CH ₃ rock, Me	oop	1034	1054			0
Q19	δ (C _{ar} -C _{ar})	rd, dir1	ip	995	1017			0.3
Q18	γ (C ₄ -C ₇ -H), δ (C ₄ -C ₇ -H _{7a})	CH ₃ wagging, Me	ip	976	996			2.8
Q17	γ (C _{ar} -H), τ (C _{ar} -C _{ar})	asym C _{ar} -H ₂ , C _{ar} -H ₃ oop bend	oop	931	954			0
Q16	γ (C _{ar} -H), τ (C _{ar} -C _{ar})	asym C _{ar} -H ₅ , C _{ar} -H ₆ oop bend	oop	903	923			0
Q15	δ _s (C _{ar} -C _{ar}), v(C _{ar} -C _{ar}), v _s (C ₁ -O ₁ ; C ₄ -C ₇)	breathing mode	ip	821	834	843	s	53
Q14	γ (C _{ar} -H), τ (C _{ar} -C _{ar})	sym C _{ar} -H ₂ , C _{ar} -H ₃ oop bend	oop	805	824	823	m	0.4
Q13	γ (C _{ar} -H), τ (C _{ar} -C _{ar})	sym C _{ar} -H ₅ , C _{ar} -H ₆ oop bend	oop	786	806			1.3
Q12	v(C ₄ -C ₇), v(C ₁ -O ₁), δ (C _{ar} -C _{ar})	C _{ar} -C and C _{ar} -O _(H) str, Me	oop	718	736	741	w	1.3
Q11	τ (C _{ar} -C _{ar}), γ (C ₁ -O ₁), γ (C _{ar} -H), γ (C ₄ -C ₇)	C ₁ , C ₃ , C ₅ up, C ₂ , C ₄ , C ₆ down	oop	674	697	701	w	2.3
Q10	δ (C _{ar} -C _{ar})	Rd	ip	632	651	645	m	7.8
Q9	γ (C ₁ -O ₁), γ (C ₄ -C ₇), τ (C _{ar} -C _{ar})	rd, sym C ₁ , C ₄ dir1	oop	498	513			0.2
Q8	δ (C _{ar} -C _{ar}),	rd dir1 C ₁ against C ₄	ip	448	463	468	m	11
Q7	δ (C ₆ -C ₁ -O ₁), δ (C ₅ -C ₄ -C ₇)	ip bend, Me	ip	410	416			0.8
Q6	τ (C _{ar} -C _{ar})	C ₃ , C ₆ up C ₂ , C ₅ down	oop	407	425			0
Q5	τ (O ₁ -H ₁)	OH torsion	oop	323	333	337	m	4
Q4	τ (C _{ar} -C _{ar}), τ (O ₁ -H ₁), γ (C ₄ -C ₇)	C ₁ -O ₁ and C ₄ -C ₇ asym oop, Me	oop	318	328			2.3

^a List of the specific vibrations and their description, the vibrational type, the calculated frequencies, the anharmonic adjusted frequencies, and the Raman intensities. The grey background is chosen for vibrations without significant contribution from the CH₃ methyl group, hence, relevant for lignin modeling.

For the H unit, the calculated data suggests that four C_{ar}H stretches constitute the three bands with two (unresolved) ip unsymmetrical stretches at $\nu_{\text{OBS}} = 3062$ cm⁻¹, and two asymmetrical stretches at 3039 cm⁻¹ and 3014 cm⁻¹.

For the G unit, the broad band at 3066 cm⁻¹ is predicted to be the two different ip stretches from C_{ar}H groups, the small band at 3040 cm⁻¹ is assigned the asymmetric stretch from C_{ar}H, and the band at 3015 cm⁻¹ arises from the stretching mode of the single ip CH of the (O)CH₃ group.

For the S unit, the band at 3062 cm⁻¹ is predicted to be the two ip C_{ar}H stretches and the intense band at 3005 cm⁻¹ is the two CH ip stretching modes of the two (O)CH₃ groups.

2980–2880 cm⁻¹. The oop unsymmetrical CH₂ stretch of the CH₃ group is predicted to give rise to the band at 2922 cm⁻¹

for the H unit, 2920 cm⁻¹ for the G unit, and 2916 cm⁻¹ for the S unit. For the (O)CH₃ groups this type of vibration is located at higher frequencies: 2940 cm⁻¹ for the G unit and 2935 cm⁻¹ for the S unit; in the latter, the band is constituted of this type of vibrations from both methoxy groups. Different CH stretches dominated by the ip CH stretch from the methyl group in all three units cannot be directly observed but may lie hidden in the broad features of the intense band(s) in the interval 2900–2950 cm⁻¹.

2880–2700 cm⁻¹. The oop symmetric CH₂ vibration from the CH₃ group shifts to a lower frequency as a function of added methoxy groups: H unit, 2867 cm⁻¹; G unit, 2842 cm⁻¹; and S unit, 2838 cm⁻¹. The symmetrical CH₃ stretch of the methoxy group in the G unit is located at 2863 cm⁻¹.

TABLE 3: Predicted and Observed Raman Data for 2-Methoxy-4-methylphenol^a

Mode	Specific atoms involved in the vibration	Details	Type	ω_{PCM} scaled (cm ⁻¹)	ω_{PCM} - ω_{AH} (cm ⁻¹)	Exp (cm ⁻¹)	I _{Raman} Exp	I _{Raman} PCM
Q54	v(O ₁ -H ₁)	ip OH str	str	3560	3492			99
Q53	v(C ₂ -H ₂)	ip CH str	str	3088	3076	3066	s	313
Q52	v(C ₅ -H ₅)	ip CH str	str	3084	3069			40
Q51	v(C ₃ -H ₃)	ip CH str	str	3067	3058	3040	w	124
Q50	v(C ₈ -H _{8b})	ip CH str	str	3047	3057	3015	m	155
Q49	v(C ₇ -H ₃)	ip asym str, Me	str	3001	3007	2965	w	97
Q48	v _a (C ₈ -H _{8a} ; C ₈ -H _{8c})	oop asym str	str	2986	2961	2940	m	74
Q47	v _a (C ₇ -H _{7b} ; C ₇ -H _{7c})	oop asym str, Me	str	2968	2939	2920	s	129
Q46	v _s (C ₈ -H ₃)	oop sym str	str	2924	2858	2863	m	292
Q45	v _s (C ₇ -H ₃)	oop sym str, Me	str	2923	2923	2842	s	225
Q44	v _s (C ₂ -C ₃ ; C ₅ -C ₆), δ (C _{ar} -H)	C _{ar} -C _{ar} str C _{ar} -H bend dir 1	ip	1599	1617	1617	s	55
Q43	v _s (C ₁ -C ₆ ; C ₃ -C ₄), δ (C _{ar} -H), δ (C ₁ -O ₁ -H ₁)	C _{ar} -C _{ar} str COH b dir 2	ip	1594	1612	1609	m	11
Q42	v(C _{ar} -C _{ar}), δ (C _{ar} -H), v _s (C ₁ -O ₁ ; C ₄ -C ₇)	C _{ar} -H ip bend and CO _(H) str and rd	ip	1498	1510	1516	w	3.6
Q41	γ (C ₈ -H ₃)	CH ₃ scissoring	oop	1468	1490			6.6
Q40	γ (C ₇ -H ₃)	CH ₃ scissoring, Me	oop	1465	1481			17
Q39	γ (C ₈ -H ₃)	CH ₃ oop bend	oop	1457	1492	1455	s	17
Q38	γ (C ₇ -H ₃)	CH ₃ oop bend, Me	oop	1452	1485			15
Q37	γ _s (C ₈ -H ₃)	CH ₃ umbrella bend	oop	1442	1444			4
Q36	γ _{s(C₈-H₃), v(C_{ar}-C_{ar}), δ(H₁-O₁-C₁), γ(C₇-H₃)}	ip bend and str, Me	ip	1407	1433	1422	w	6.7
Q35	γ _{s(C₇-H₃)}	umbrella bend	oop	1385	1448	1379	s	30
Q34	δ (H ₁ -O ₁ -C ₁), v(C _{ar} -C _{ar})	COH ip bend and rd	ip	1358	1373	1363	m	16
Q33	δ (C _{ar} -H), δ (C ₁ -O ₁ -H ₁)	rd and ip C _{ar} -H and COH bend	ip	1281	1302	1288	s	7.8
Q32	v(C _{ar} -C _{ar}), v _s (C ₁ -O ₁ ; C ₆ -O ₂), δ (C _{ar} -H)	rd and CO _(H) str	ip	1254	1274	1272	s	25
Q31	δ (C _{ar} -C _{ar}), δ (C _{ar} -H ₅), δ (C _{ar} -H ₃), δ (C ₁ -O ₁ -H ₁), v(C ₁ -O ₁)	C-O _(H) str, COH ip bend and rd	ip	1219	1237	1241	w	2.1
Q30	δ _{s(O₂-C₈-H_{8b}; C₁-O₁-H₁)}	(O)CH ₃ wagging and COH ip bend	ip	1188	1213	1208	m	9.6
Q29	δ _{a(O₂-C₈-H_{8b}; C₁-O₁-H₁)}	(O)CH ₃ wagging and COH ip bend	ip	1170	1190	1186	s	13
Q28	δ (O ₂ -C ₈ -H _{8b}), v _s (C ₆ -O ₂ ; C ₈ -O ₂), δ _{s(C₃-C₂-H₂; C₄-C₅-H₅), δ(C₁-O₁-H₁), v(C₄-C₇)}	ip C _{ar} -H bend, OCH and COH bend, C _{ar} OC asym str	ip	1138	1161	1155	w	1.2
Q27	γ (C ₈ -H)	(O)CH ₃ oop twist	oop	1137	1154			2.3
Q26	δ _{s(C₃-C₂-H₂; C₂-C₃-H₃)}	C _{ar} -H ip bend H ₂ towards H ₃	ip	1109	1139	1122	w	1
Q25	γ (C ₇ -H ₃)	Me oop rock	oop	1032	1048	1036	w	0.1
Q24	v(O ₂ -C ₈), δ (C _{ar} -C _{ar})	ip rd and O-C _(H3) str	ip	1025	1041			3.8
Q23	γ (C ₇ -H ₃)	Me ip wagging	ip	993	1017			3.4
Q22	γ _{a(C₃-H₃; C₂-H₂)}	asym oop CH bend	oop	905	930			0.1
Q21	δ (C ₂ -C ₃ -C ₄), v(C ₄ -C ₇), v(C ₆ -O ₂), v(C ₈ -O ₂)	rd and ip C-C _(H3) str and COC str	ip	900	923	921	m	15
Q20	γ (C ₅ -H ₅)	CH oop bend	oop	828	840			0.2
Q19	γ _{s(C₃-H₃; C₂-H₂)}	CH oop bend	oop	794	813	793	s	1.6
Q18	δ (C ₄ -C ₅ -C ₆), v(C ₁ -O ₁)	rd and C-O _(H) str	ip	777	796			25
Q17	δ (C ₁ -C ₂ -C ₃), v(C ₄ -C ₇)	rd and C _{ar} -C _(H3) str	ip	694	711	712	s	13
Q16	τ (C _{ar} -C _{ar})	sym up C ₂ ,C ₄ ,C ₆ oop and sym down	oop	686	718			0.8
Q15	τ (C _{ar} -C _{ar})	rd C ₄ oop	oop	573	586	590	w	0.5
Q14	δ _{a(O₁-C₁-C₂; C₅-C₄-C₇)}	C _{ar} C _{ar} O _(H) and C _{ar} C _{ar} C _(H3) ip bend	ip	540	552	559	m	6.1
Q13	δ _{a(C₆-O₂-C₈; C₃-C₄-C₇), δ(C_{ar}-C_{ar})}	C _{ar} OC and C _{ar} C _{ar} C _(H3) ip bend and rd	ip	530	544	541	w	3.1
Q12	δ _{s(C₂-C₁-C₆; C₃-C₄-C₅)}	rd C ₁ towards C ₄	ip	450	460	468	m	11
Q11	τ (C _{ar} -C _{ar}), τ (O ₁ -H ₁)	oop OH torsion and ar. torsion	oop	442	458			0.9
Q10	τ (O ₁ -H ₁)	oop OH torsion	oop	421	366			0.6
Q9	δ _{s(C₈-O₂-C₆; C₇-C₄-C₃; C₆-C₁-O₁)}	ip substituent bend	ip	351	359	370	w	3.4
Q8	τ CCO _(H) , τ CCO _(OMe) , τ CCC _(Me)	ar-substituents torsion	oop	344	343	357	m	3.3

^a List of the specific vibrations and their description, the vibrational type, the calculated frequencies, the anharmonic adjusted frequencies, and the Raman intensities; ν stretch; γ oop bend; δ ip bend; τ torsion. The grey background is chosen for vibrations without significant contribution from the CH₃ methyl group, hence, relevant for lignin modeling.

For the S unit there are two different CH₂ symmetrical stretches of the (O)CH₃ group giving rise to the 2859 cm⁻¹ band. Calculations predict three CH₂ symmetrical vibrations to be in the range 2924–2915 cm⁻¹, suggesting that the bands are difficult to separate. Correcting the vibrations with the

anharmonic contributions gave the following frequencies: Modes from the (O)CH₃ groups at 2854 cm⁻¹ and 2866 cm⁻¹ and the mode from the CH₃ methyl group at 2923 cm⁻¹. The anharmonic contribution results suggest that the two methoxy group vibrations have similar frequencies and, therefore,

TABLE 4: Predicted and Observed Raman Data for 2,6-Dimethoxy-4-methylphenol^a

Mode	Specific atoms involved in the vibration	Description	Type	0° (cm ⁻¹)		120° (cm ⁻¹)		Exp (cm ⁻¹)	I _{Raman, Exp}	I _{Raman, PCM 0°}	I _{Raman, PCM 120°}
				ω_{PCM} scaled	$\omega_{PCM} - \omega_{AH}$	ω_{PCM} scaled	$\omega_{PCM} - \omega_{AH}$				
Q66	v(O ₁ -H ₁)	ip OH str	str	3564	3521	3557	3515			106	101
Q65	v(C ₃ -H ₃)	ip CH str	str	3098	3083	3090	3086		m	132	117
Q64	v(C ₅ -H ₅)	ip CH str	str	3095	3091	3081	3070	3062		83	140
Q63	v(C ₈ -H _{8c})	ip CH str	str	3046	3057	3048	3055	3005	m	164	157
Q62	v(C ₉ -H _{9c})	ip CH str	str	3041	3052	3039	3026			175	148
Q61	v _s (C ₇ -H _{7a} ; C ₇ -H _{7c})	oop asym str, Me	str	2999	2994	3004	2972			92	93
Q60	v _s (C ₈ -H _{8b} ; C ₈ -H _{8a})	oop asym str	str	2986	2959	3002	2977	2935	s	78	92
Q59	v _s (C ₇ -H ₃)	oop asym str, Me	str	2974	2943	2988	2991			157	76
Q58	v _s (C ₉ -H _{9b} ; C ₉ -H _{9a})	oop asym str	str	2974	2921	2970	2941	2916	s	52	133
Q57	v _s (C ₈ -H ₃)	oop sym str	str	2924	2866	2926	2861	2859	s	231	356
Q56	v _s (C ₇ -H ₃)	oop sym str, Me	str	2922	2923	2924	2857	2838	s	330	330
Q55	v _s (C ₉ -H ₃)	oop sym str	str	2915	2854	2924	2921	2859	s	180	32
Q54	v _s (C ₁ -C ₂ ; C ₄ -C ₅)	C _{ar} -C _{ar} sym str COH bend dir2	ip	1600	1620	1596	1617	1609	s	9.1	41
Q53	v _s (C ₂ -C ₃ ; C ₅ -C ₆)	C _{ar} -C _{ar} sym str C _{ar} H bend dir1	ip	1586	1606	1589	1610			83	32
Q52	v _s (C ₁ -C ₂ ; C ₆ -C ₁), v _s (C ₁ -O ₁), δ (C _{ar} -H)	C _{ar} H ip bend and CO _(H) str and rd	ip	1501	1518	1487	1512	1516	w	2.6	3.9
Q51	γ (C ₈ -H ₃)	CH ₃ scissoring	oop	1468	1488	1473	1481			13	12
Q50	γ (C ₉ -H ₃)	CH ₃ scissoring	oop	1468	1479	1468	1488	1465	m	11	17
Q49	γ (C ₇ -H ₃)	CH ₃ oop bend	oop	1465	1486	1465	1483			6.6	3.6
Q48	γ (C ₉ -H ₃)	CH ₃ oop bend	oop	1458	1499	1456	1491			18	17
Q47	γ (C ₈ -H ₃)	CH ₃ oop bend	oop	1456	1486	1452	1471	1452	m	20	14
Q46	γ (C ₇ -H ₃)	CH ₃ scissoring	oop	1454	1452	1451	1453			14	15
Q45	γ (C ₈ -H ₃)	Umbrella bend	oop	1443	1463	1442	1472			6.5	4.4
Q44	γ (C ₉ -H ₃)	Umbrella bend	oop	1442	1467	1437	1445			2.5	9.9
Q43	v _s (C ₂ -C ₃ ; C ₅ -C ₆), v _s (C ₈ -H ₃), v _s (C ₉ -H ₃), δ (C _{ar} -H), δ (H ₁ -O ₁ -C ₁)	rd, (O)CH ₃ umbrella vibration, ip COH bend	oop	1408	1437	1403	1426	1422	w	11	8
Q42	γ (C ₇ -H ₃)	Umbrella bend	oop	1384	1451	1384	1450	1379	m	33	31
Q41	δ (H ₁ -O ₁ -C ₁), v(C _{ar} -C _{ar})	COH ip bend and rd	ip	1353	1366	1356	1374			3.5	26
Q40	v _s (C ₆ -O ₂ ; C ₂ -O ₃ ; C ₄ -C ₇), v(C _{ar} -C _{ar})	rd and C _{ar} OC str	ip	1315	1336	1291	1309	1331	s	42	39
Q39	δ (C ₁ -O ₁ -H ₁), δ (C _{ar} -H)	COH and CH ip bend	ip	1264	1288	1247	1267	1316	w	1.5	1.2
Q38	δ (C _{ar} -H ₃), v(C ₁ -O ₁), δ (C _{ar} -C _{ar})	CO _(H) str and C _{ar} H ₇ ip bend	ip	1227	1246	1222	1244	1241	w	5.5	1.6
Q37	δ (C _{ar} -H ₃), δ (C ₁ -O ₁ -H ₁)	COH ip bend and C _{ar} H ₃ ip bend	ip	1201	1220	1197	1218	1214	w	1.8	7.5
Q36	δ _s (O ₂ -C ₈ -H ₃ ; O ₃ -C ₉ -H ₃)	(O)CH ₃ ip wagging	ip	1176	1194	1177	1196		m	3.6	5.5
Q35	δ _s (O ₂ -C ₈ -H ₃ ; O ₃ -C ₉ -H ₃)	(O)CH ₃ ip wagging	ip	1171	1185	1172	1193	1187		7.6	5.4
Q34	v(C ₄ -C ₇), δ (C _{ar} -H ₃ ; C _{ar} -H ₅)	C _{ar} H ip bend	ip	1144	1170	1137	1158			8.2	2.2
Q33	γ (O ₂ -C ₈ -H ₃)	(O)CH ₃ oop rock	oop	1136	1146	1136	1156	1152	w	2.6	3.6
Q32	γ (O ₃ -C ₉ -H ₃)	(O)CH ₃ oop rock	oop	1135	1160	1132	1155			2.1	2.4
Q31	δ (H ₁ -O ₁ -C ₁), v _s (C ₈ -O ₂ ; C ₃ -O ₃), v _s (C ₈ -O ₂ ; C ₆ -O ₂)	COH ip bend and OC _(H) str	ip	1110	1119	1088	1101	1116	w	2	2.9
Q30	v _s (C ₈ -O ₂ ; C ₉ -O ₃), δ (C _{ar} -C _{ar})	OC _(H) str and rd	ip	1038	1051	1031	1043	1043	s	12	0.3
Q29	γ (C ₇ -H ₃)	CH ₃ wagging	oop	1027	1048	1026	1047			4.9	25
Q28	γ (C ₇ -H ₃)	CH ₃ oop bend	oop	999	1016	995	1020			2.1	1.9
Q27	v(C ₄ -C ₇), δ (C _{ar} -C _{ar}), v _s (C ₈ -O ₂ ; C ₆ -O ₂ ; C ₈ -O ₃ ; C ₂ -O ₃)	rd and C _{ar} C str	ip	946	964	930	943	966	w	5.9	6.3
Q26	δ (C _{ar} -C _{ar}), δ (C ₁ -O ₁ -H ₁), v _s (C ₈ -O ₂ ; C ₆ -O ₂), v _s (C ₈ -O ₃ ; C ₂ -O ₃)	rd and ip COH bend and COC _{ar} str	ip	888	899	895	908	907	w	1.6	1.8
Q25	γ (C _{ar} -H)	H ₃ and H ₅ asym oop	oop	806	818	844	861			0.9	0.4
Q24	γ (C _{ar} -H)	H ₃ and H ₅ sym oop	oop	789	808	806	809			1.6	0.5
Q23	δ (C _{ar} -C _{ar}), v(C ₉ -C ₄)	rd, CO _(H) str	ip	781	800	773	790	799	s	27	24
Q22	π (C _{ar} -C _{ar})	C ₂ , C ₄ , C ₆ up, C ₁ , C ₃ , C ₅ down	oop	698	743	715	747			0.2	0.4
Q21	δ _s (C ₅ -C ₆ -O ₂ ; C ₃ -C ₂ -O ₃), δ _s (C ₅ -C ₄ -C ₇ ; C ₆ -C ₁ -O ₁)	all substituent ip bend	ip	629	643	636	667			0.2	1.9
Q20	π (C _{ar} -C _{ar})	rd asym C ₂ , C ₆ oop	oop	567	558	595	605	582	s	2.5	1.3
Q19	π (C _{ar} -C _{ar}), δ (C ₈ -O ₂ -C ₆ ; C ₈ -O ₃ -C ₂), v(C ₄ -C ₇)	rd C ₃ , C ₆ out, C ₂ , C ₄ in	oop	564	573	575	579			8.4	0.4
Q18	π (C _{ar} -C _{ar})	C ₄ in and oop	oop	557	555	541	549	564	m	3	12
Q17	δ (C _{ar} -C _{ar})	rd C ₃ towards C ₆	ip	517	532	502	514	529	w	5.4	10
Q16	δ (C _{ar} -C _{ar}), δ _s (C ₈ -O ₂ -C ₆ ; C ₉ -O ₃ -C ₂)	rd C ₁ towards C ₄	ip	450	453	442	450			11	6.6
Q15	π (O ₁ -H ₁)	oop OH torsion	oop	432	407	429	397			1.4	1.5
Q14	δ _s (C ₈ -O ₂ -C ₆ ; C ₉ -O ₃ -C ₂), δ (C ₅ -C ₄ -C ₇)	asym C _{ar} OC ip bend	ip	367	374	388	389			0	1.8
Q13	δ (C ₈ -O ₂ -C ₆ ; C ₉ -O ₃ -C ₂)	sym C _{ar} OC ip bend	ip	353	359	358	347	369	s	11	3.9
Q12	γ (C _{ar} -C ₄ -C ₇ ; C _{ar} -C ₁ -O ₁)	sym up: C ₃ , C ₄ , C ₅ , O ₁ sym down: C ₆ , C ₁ , C ₂ and C ₇	oop	347	339	311	324			2	4.2

^a List of the specific vibration and their description, the vibrational type, the calculated frequencies, the anharmonic adjusted frequencies, and the Raman intensities for both conformations; ν stretch; γ oop bend; δ ip bend; π torsion. The grey background is chosen for vibrations without significant contribution from the CH₃ methyl group, hence, relevant for lignin modeling.

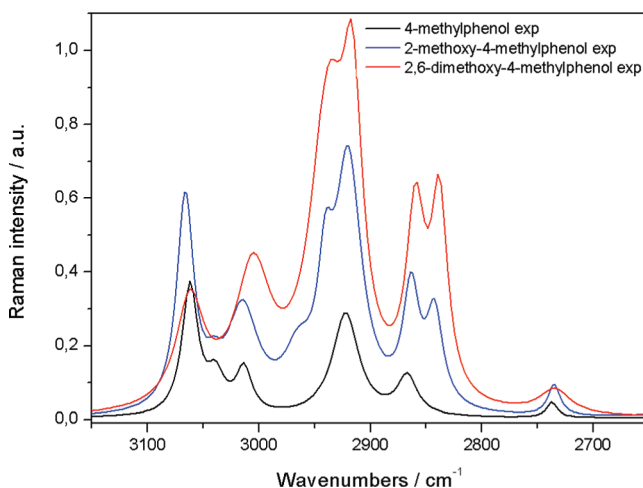


Figure 4. Experimental spectra of 4-methylphenol, 2-methoxy-4-methylphenol, and 2,6-dimethoxy-4-methylphenol. Displayed is the sp^3 hybridized and sp^2 hybridized CH stretching region.

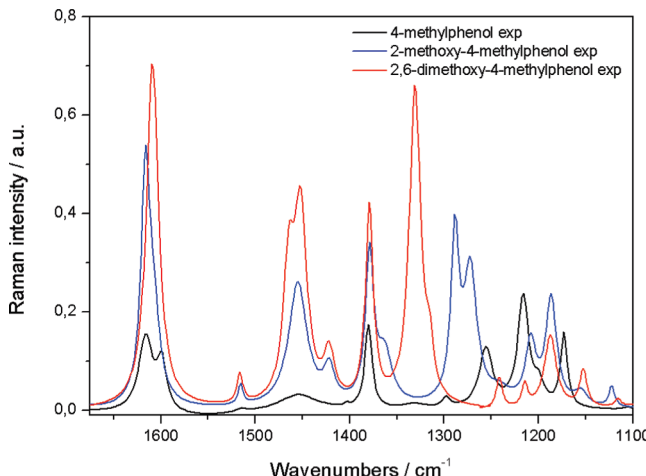


Figure 5. Experimental spectra of 4-methylphenol, 2-methoxy-4-methylphenol, and 2,6-dimethoxy-4-methylphenol. Displayed is the interval $1675\text{--}1100\text{ cm}^{-1}$.

constitute the single band observed in the experimental spectrum at 2859 cm^{-1} .

The band at 2730 cm^{-1} is for all three molecules assigned the well-known overtone of the CH_3 1379 cm^{-1} umbrella vibration.

In Figure 5, the interval from 1700 to 1100 cm^{-1} is shown.

1650–1550 cm⁻¹. In the interval between 1650 and 1550 cm^{-1} , one or two overlapping bands are observed for all units. According to the calculations, two different aromatic ring deformations are responsible for this band, which is thus a two-component band for all three lignin model monomers. The calculated differences in frequency are 24 cm^{-1} (H), 5 cm^{-1} (G), and 14 cm^{-1} (S), and the corresponding calculated Raman activity ratios are (high wavenumber/low wavenumber) 4:1 (H), 5:1 (G), and 1:9 (S). These two modes can be described as two different $\text{C}_{\text{ar}}-\text{C}_{\text{ar}}$ stretches; one compressing the benzene ring in the direction aligned with the hydroxy $\text{C}-\text{O}_{(\text{H})}$ bond (direction 1) and one compressing the benzene ring along two other $\text{C}_{\text{ar}}-\text{C}_{\text{ar}}$ (direction 2). These bands show a predicted *opposite* positional shift as a function of adding methoxy groups, $\text{C}_{\text{ar}}-\text{C}_{\text{ar}}$ (dir. 1), 1606 cm^{-1} (H) \rightarrow 1599 cm^{-1} (G) \rightarrow 1586 cm^{-1} (S); and for the $\text{C}_{\text{ar}}-\text{C}_{\text{ar}}$ (dir. 2), 1582 cm^{-1} (H) \rightarrow 1594 cm^{-1} (G) \rightarrow 1600 cm^{-1} (S). Also, the intensity difference increases as a function of adding methoxy groups. These predictions are in

good accordance with the observed two distinct bands of the H unit, a broad asymmetrical band of the G unit, and an apparent single band of the S unit.

1550–1500 cm⁻¹. At 1515 cm^{-1} , a weak band is observed for all three models. This mode is dominated for all three compounds by an ip $\text{C}_{\text{ar}}\text{H}$ bend in combination with $\text{C}_{\text{ar}}-\text{O}_{(\text{H})}$ stretch and ring deformation.

1500–1400 cm⁻¹. One broad and one narrow band is observed for the H unit, two broad bands for the G and S unit, as well as a weak shoulder for the S unit.

The calculations predict for the H unit two different oop CH bends (scissoring) from the CH_3 group at 1464 cm^{-1} and 1453 cm^{-1} . A ring deformation mode is predicted at 1413 cm^{-1} for the H unit and gives rise to the low intensity band seen at 1403 cm^{-1} .

For the G unit, the same two types of CH bending vibrations as for the H unit exist both for the CH_3 and $(\text{O})\text{CH}_3$ groups. In addition, a weak $(\text{O})\text{CH}_3$ umbrella bending vibration also occurs. These five modes are placed within a predicted range of 26 cm^{-1} , giving the broad band at 1460 cm^{-1} displayed in the experimental spectrum. The less intense broad band at 1422 cm^{-1} corresponds with a single predicted aromatic ip deformation mode.

For the S unit, three bands are observed at 1465 , 1452 , and 1422 cm^{-1} . The calculated data predicts two oop CH_2 bending vibrations from each CH_3 group, three of which lies within a predicted range of 3 cm^{-1} , assigned to the band at 1465 cm^{-1} , and the other three within a predicted range of 4 cm^{-1} assigned to the band at 1452 cm^{-1} . Besides these six vibrations, two weak umbrella vibrations from the two $(\text{O})\text{CH}_3$ groups are predicted, but they cannot be discerned from the CH_3 vibrations. The band at 1422 cm^{-1} is the ring deformation also predicted for the H and G unit.

1400–1350 cm⁻¹. In the interval $1400\text{--}1350\text{ cm}^{-1}$ a single band is observed for the H and S unit and two bands for the G unit. The intense band at 1379 cm^{-1} is for all three assigned the CH_3 umbrella vibration. The shoulder observed for the G unit at 1363 cm^{-1} is predicted to be an ip $\text{C}_{\text{ar}}\text{OH}$ bend in combination with an aromatic deformation and is predicted to occur at 1358 cm^{-1} (frequency scaled). The same type of vibration is also predicted for the H unit and the S unit at 1321 and 1353 cm^{-1} , respectively, but with intensities suggesting that they are not observable.

1350–1100 cm⁻¹. In the interval from 1320 to 1100 cm^{-1} six bands are observed for the H unit. The very weak band at 1298 cm^{-1} corresponds to ring deformation and ip bending, the band at 1256 cm^{-1} corresponds to CO stretch and ip bending, and the band at 1216 cm^{-1} corresponds to ring deformation, $\text{C}_{\text{ar}}\text{CH}_3$, and $\text{C}_{\text{ar}}\text{H}$ ip bending. The shoulder at 1199 cm^{-1} is assigned ip $\text{C}_{\text{ar}}\text{H}$ bending, the band at 1173 cm^{-1} is assigned to $\text{C}_{\text{ar}}\text{OH}$ ip bending, and the very weak band at 1105 cm^{-1} is assigned to a complex ip bending vibration.

For the G unit seven bands have been determined from Lorentz fitting of the experimental spectrum. The intense band at 1288 cm^{-1} is caused by ring deformation and ip COH bending. The band at 1272 cm^{-1} is assigned to a ring deformation. The weak shoulder at 1241 cm^{-1} is assigned CO stretching, ip bending, and ring deformations. The bands at 1208 cm^{-1} and 1186 cm^{-1} are symmetric and asymmetric $\text{O}-\text{CH}_3$ wagging combined with the $\text{C}_{\text{ar}}-\text{O}-\text{H}$ ip bending. The band at 1155 cm^{-1} is assigned two different vibrations: an ip complex vibration and an oop CH_3 twisting vibration. Both are calculated to be low in intensity and only separated by 1 cm^{-1} . The band at 1122 cm^{-1} is assigned a $\text{C}_{\text{ar}}\text{H}$ ip bending mode.

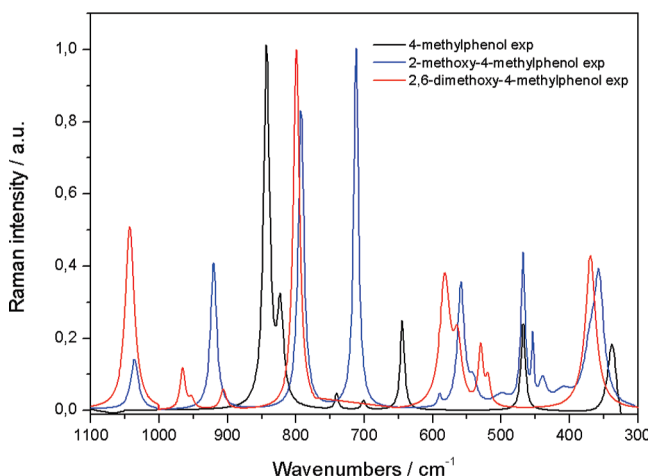


Figure 6. Experimental spectra of 4-methylphenol, 2-methoxy-4-methylphenol, and 2,6-dimethoxy-4-methylphenol. Displayed is the interval 1100–300 cm⁻¹.

For the S unit an intense peak is observed at 1331 cm⁻¹. This band is assigned a ring deformation, best described as a ring deformation mode, coupled with COC stretches of the two (O)CH₃ groups. The shoulder that appears to the right of this band is from a combination of COH ip bend and C_{ar}H ip bend. The band at 1241 cm⁻¹ is dominated by C_{ar}O_(H) stretch, and the band at 1214 cm⁻¹ is caused by a COH ip bend. The band at 1187 cm⁻¹ is predicted to be two overlapping vibrations from (O)CH₃ wagging, one from each (O)CH₃ group. The band at 1152 cm⁻¹ can be assigned from the calculational data to be a combination of three modes: ip C_{ar}H bending with the main intensity contribution and two different (O)CH₃ rocking vibrations. The weak band at 1116 cm⁻¹ is dominated by COH ip bend.

In Figure 6, the 1100–300 cm⁻¹ interval of the Raman spectra is shown.

In this interval caution should be taken regarding artifacts from subtraction of the CCl₄ spectrum. It displays a doublet at 789 and 761 cm⁻¹ (not shown), which due to its weakness can be subtracted with no problems. The intense CCl₄ band at 460 cm⁻¹ is not equally straightforward to subtract, and therefore, the interval 420–500 cm⁻¹ is considered with caution, whereby only the intense bands at 468 cm⁻¹ for the H and G unit are considered.

1100–900 cm⁻¹. In this interval no bands are observed for the H unit. Five modes are predicted, all of very low intensity, explaining their absence in the Raman spectrum.

The spectrum of the G unit displays two bands at 1036 and 921 cm⁻¹. The first band is predicted to be an ip ring deformation and O–CH₃ stretching mode. A very weak mode dominated by methyl group vibrations is predicted in close vicinity but is not observed in the spectrum. The second band at 921 cm⁻¹ is an aromatic deformation mode. Besides these, two other modes, an asymmetric C_{ar}H mode and a CH₃ wagging vibration are predicted both with very low intensity.

The spectrum of the S unit shows four bands in this interval. The band at 1043 cm⁻¹ is predicted to be two overlapping modes: one dominated by symmetric stretch of the O–C bond in the two OCH₃ groups and the second a CH₃ wagging vibration. The first mode is predicted to contribute the most to the intensity (intensity ratio = 12:5). The band observed at 966 cm⁻¹ is predicted to be a ring deformation in combination with a C_{ar}CH₃ stretching vibration. The band at 953 cm⁻¹ cannot be explained from the calculated data, but may be a combination

band of the intense vibrations at 582 and 369 cm⁻¹. The band at 907 cm⁻¹ is assigned a complex ip ring deformation. A band is also predicted at 1000 cm⁻¹ but with too low intensity to be observed.

900–660 cm⁻¹. For the H unit four bands are observed. A very intense band at 843 cm⁻¹ assigned the aromatic breathing mode, and a medium intense band at 823 cm⁻¹, unexplained by the calculated data. A weak band is observed at 741 cm⁻¹ and is caused by an asymmetric C_{ar}–C_(H3) and C_{ar}–O_(H) stretch mode and a band at 701 cm⁻¹ is assigned an oop ring deformation mode.

Two intense bands are observed for the G unit at 793 cm⁻¹ and 712 cm⁻¹. These are oop ring deformation modes in combination with a C_{ar}–O_(H) stretch or a C_{ar}–C_(H3) stretch, respectively, for the higher and lower frequency mode. Three other modes are predicted, all with very low Raman activities.

One band is observed for the S unit at 799 cm⁻¹ and is assigned a combination of ring deformation and a dominating C_{ar}–O_(H) stretch. Three other bands of low intensity are predicted in this interval.

660–300 cm⁻¹. Three medium intense bands are observed for the H unit. The bands at 645 and 468 cm⁻¹ are caused by ip ring deformation modes, and the band at 337 cm⁻¹ is caused by two close lying modes, with a predicted main contribution from the OH torsion mode. Six other bands are predicted, all with very low intensity, and are thus not observed.

For the G unit 10 bands can be observed. However, the spectrum of CCl₄ displays intense bands at 400–500 cm⁻¹, and therefore, four apparent bands are artifacts from the subtraction of the solvent spectrum, which leaves six real bands. The band at 590 cm⁻¹ is an oop ring deformation. The band at 559 cm⁻¹ is an ip ring deformation in combination with a dominating C_{ar}–OH ip bend. The band at 541 cm⁻¹ is an ip ring deformation dominated by an ip C_{ar}–O–C_(H3) bend. The medium intense band at 468 cm⁻¹ is a symmetric ring deformation involving mainly the ring carbon atoms with the substituent OH and CH₃. The two overlapping bands at 370 and 357 cm⁻¹ are, respectively, assigned a symmetric ip bend of the three substituents, and an oop torsional mode around the ring center as seen for the H unit. Nine other modes are predicted, but all are very weak and therefore not observed.

Five bands are observed for the S unit. The band at 582 cm⁻¹ is caused by two modes separated by 3 cm⁻¹, and the band at 564 cm⁻¹ is a single mode, all three of which are oop ring deformation modes. The band at 564 cm⁻¹ appears asymmetrical toward the low frequencies. This can be explained as a consequence of the increase in intensity for this band in the 120° conformer, for which the Q18 vibration is down shifted 16 cm⁻¹ (freq scaled). The band at 529 cm⁻¹ is assigned an ip ring deformation. The weaker band observed at 519 cm⁻¹ can likewise be explained by the 120° conformer for which the same vibration (Q17) is predicted with a harmonic frequency shift of ~15 cm⁻¹ (freq scaled). This conformer has a significant population probability (see Table 1), and the Raman activity for this mode is doubled as compared to the 0° conformation. Finally, the band at 369 cm⁻¹ is assigned a symmetric ip bend of the C_{ar}–O–C_(H3) of the two methoxy groups. Furthermore, 16 predicted bands could not be assigned to the experimental spectrum due to low Raman activity.

Accuracy. Root mean square (rms) error values of predicted versus observed frequencies have been calculated for all normal modes that could be assigned bands in the experimental spectra. In Table 5 the rms error values for the four different models are displayed. They are divided into *all* vibrations, and the three

TABLE 5: Average RMS Errors from the Experimental and Predicted Raman Data of the Lignin Model Monomers: 4-Methylphenol, 2-Methoxy-4-methylphenol, and the Two Conformations of 2,6-Dimethoxy-4-methylphenol^a

Compound/Type	all _{AH}	all _f	ip _{AH}	ip _f	oop _{AH}	oop _f	str _{AH}	str _f	all* _{AH}	Oop* _{AH}
4-methylphenol	28	27	15	19	31	20	41	44	24	18
2-methoxy-4-methylphenol	24	25	7	16	29	12	35	45	21	21
2,6-dimethoxy-4-methylphenol 0°	25	29	10	19	27	12	37	52	23	19
2,6-dimethoxy-4-methylphenol 120°	25	33	17	27	24	14	36	55	23	16
Average	25	28	11	19	28	14	37	48	22	19
Number of fundamentals		110		49		35		26	106	31

^a RMS values determined from anharmonic corrected predicted values (AH) and factor corrected predicted values (f). The * indicates RMS values determined by neglecting the umbrella CH₃ vibration, experimentally found at 1379 cm⁻¹. The grey background is chosen for vibrations without significant contribution from the CH₃ methyl group, hence, relevant for lignin modeling.

different types of vibrations, that is, vibrations >2500 cm⁻¹, ip vibrations (<2500 cm⁻¹), and oop vibrations (<2500 cm⁻¹). The error values have also been determined for “all vibrations” and “oop vibrations”, leaving the troublesome CH₃ umbrella vibration out, indicated by a *. A further division is made in terms of the method of either harmonic frequency scaling or explicit anharmonic frequency shift correction denoted as “f” and “AH” subscripts, respectively.

Discussion

From Table 5 it is clear that the >2500 cm⁻¹ CH stretch region shows large errors regardless of the method used. Raman activities and band forms are not well predicted either.

Frequencies of the ip type vibrations are best predicted by explicit correction for anharmonicities, where an overall rms error of 11 cm⁻¹ is obtained, whereas oop vibrations are better predicted using the scaling factor approach, with an overall error of 14 cm⁻¹. At relatively low $T \leq 300$ K the conformer probability was predicted to be biased toward the 0° conformation, and with a few exceptions, it is the normal modes of this conformer that best represent this lignin model monomer. The frequency prediction errors for the ip normal modes <2500 cm⁻¹ show this tendency. The exceptional normal modes are “counter-biased” by their relatively large intensity gain for the 120° conformer, that is, the Q17, Q18, Q41, and Q54 modes (see Table 4). For Q17 and Q18 a relatively large frequency shift is also predicted, whereby they could each tentatively be assigned a 0° and 120° conformer bands.

Caution should be taken with some types of vibrations. The anharmonic contribution to the CH₃ umbrella vibrations at 1379 cm⁻¹ is problematic and neglecting this vibration causes the rms error to decrease from 28 to 19 cm⁻¹ for the oop AH vibrations. Considering this, as well as ignoring the high frequency region, good predictions can thus be obtained.

A significant part of the errors obtained is likely due to the limited size 6-31+G(d) basis set used, which is a compromise between computational efficiency and accuracy, where the diffuse functions on O and C serve to (also) give reasonable Raman intensities. Whereas the CH₃ umbrella vibrations are not

relevant in the context of modeling lignin, which always has a basic three-carbon C–C–C substitution in place of the methyl group, other oop vibrations are relevant. These are, for example, vibrations with significant contributions of C_{ar}H oop bending and oop ring distortions. For phenol, such vibrations can require basis sets of at least triple- ζ quality (e.g., aug-cc-pVTZ) to make harmonic frequency basis set errors insignificant, say <5 cm⁻¹.³⁷ The same types of vibrations are found for the three lignin models, and it is thus likely that the limited size basis set and the B3LYP method are both significant error sources. The basis set dependency of the HF anharmonic shifts for the lignin model models is not known, and a significantly larger basis set for this calculation is practically infeasible. However, as these shifts are generally a factor of ~20 smaller than the harmonic frequency a much larger relative (%) error in their prediction is tolerable. Further improvement of the methods used in the present work should focus on the method (functional) and the basis set used for harmonic frequency calculation.

Besides the rather poor possibility of assigning the bands in the interval above 2500 cm⁻¹, the whole CH stretch region depicted in Figure 3 does not show marked differences between the H, G, and S units and is, thus, of limited use if particular H, G, or S (phenolic) “marker bands” are sought. The most information that can be gained is that, if the spectrum displays two bands around ~2850 and ~2920 cm⁻¹, the S and G unit types are present.

The low frequency interval 1700–300 cm⁻¹ is more promising for locating marker bands. If the spectrum displays intense peaks around 1455 cm⁻¹, the lignin monomer model contains OCH₃ groups (the band is caused by CH₃ oop vibration from the OCH₃ group). If a doublet is present at 1455 cm⁻¹, it is caused by the two different OCH₃ groups and can be used as a direct marker band for S-units. The intense band at 1331 cm⁻¹ from a ring deformation coupled with symmetric C–O_(CH₃) stretches is a prominent marker band for the S unit. As a marker band for the G unit, the medium intense doublet present in the interval 1250–1300 cm⁻¹ can be used. These bands are caused by a ring deformation coupled with ip C_{ar}H bends (1288 cm⁻¹) and from a ring deformation coupled with symmetric C–O

stretches. The intense band at 843 cm^{-1} from the ring breathing mode is a strong marker band for the H unit and probably the only significant one if the H units exist together with G and S units.

A doublet of intense bands at 700 and 800 cm^{-1} caused by two different ring deformations can be used as marker for the G units, whereas the S units only display one intense band, overlapping with the band from the G unit at approximately 800 cm^{-1} .

Besides the use of electronic structure methods for locating marker bands, other information can also be obtained. An interesting effect of methoxy substitution $\text{H} \rightarrow \text{G} \rightarrow \text{S}$ can be demonstrated. Especially the double band at 1600 cm^{-1} is interesting.

Previously this double band character has been overlooked and only a single band was assigned lignin or lignin models.^{16,7} The new knowledge that the $\sim 1600\text{ cm}^{-1}$ band is composed of two different aromatic ip stretches is likely generally valid for all lignin aromatic structures as these exhibit the same ring substitution pattern as the phenols examined in the present work. This knowledge could, for example, be used in combination with polarized Raman spectroscopy. Previously, Atalla and Agarwal³⁸ studied lignin orientation in cell walls of native woody tissue. This was done using the $\sim 1600\text{ cm}^{-1}$ band to investigate the lignin orientation in relation to the cell wall. By analyzing this band in terms of its polarization components more detailed information may be retrieved regarding the orientation of the lignin polymer, that is, the alignment of S and G units, the difference between wood species, and so on. An alternative investigation is to monitor the photo degradation of softwood and hardwood using this information. Hardwood is degraded faster than softwood.³⁹ Monitoring the band shapes as function of exposure time of UV light in hardwood could give information on the distribution of S and G units and the specific rate of their degradation. This knowledge also offers a route to study the DHP polymerization process. Many studies have been performed on the in vitro formation of lignin.^{40–44} Following the intensity increase of these specific bands in a process where both coniferyl alcohol and sinapyl alcohol are used could give information on the rate and chronology of the polymerization.

Another advantage of doing calculations is that they can clarify what types of vibrations are seen in the Raman spectra. For example, in the interval from 1320 to 1100 cm^{-1} the band observed in the spectrum of the H unit at 1216 cm^{-1} corresponds to a ring deformation, with minor contributions from $\text{C}_{\text{ar}}\text{CH}_3$ and $\text{C}_{\text{ar}}\text{H}$ ip bending: This is opposed to the assignment, aryl–O–R (R = H or CH_3) vibration, given by Agarwal⁴⁵ and Saariaho et al.¹⁶ This is also the case for the S units' intense peak at 1331 cm^{-1} . Saariaho et al¹⁶ discuss the assignment of this band. Their investigation of the three S-type units, 4-methyl-2,6-dimethoxyphenol, 3,5-dimethoxy-4-hydroxy-benzaldehyde, and 3,4,5-trimethoxytoluene, shows an intense UV resonance Raman (UVRR) band for all three units. By the UVRR study of the 1331 cm^{-1} vibration, they dismiss the argument of Agarwal⁴⁵ that the vibration is caused by aliphatic–O–H bend. Because the bands were resonance enhanced, they therefore suggested that the vibration could arise from aryl–O–CH₃ structures. Our calculations show unequivocally this band to arise from a ring deformation, best described as an asymmetric breathing mode, coupled with CO stretching of the methoxy groups.

Though, not all observed bands correspond to predicted calculations. For example the band of the H unit at 823 cm^{-1} can be explained only by invoking the effect of Fermi resonance.

This H-unit doublet (i.e., the 823 and 843 cm^{-1} bands) is well characterized because 4-methylphenol is a common model of the tyrosine side chain in proteins.^{46–48} For tyrosine, the Fermi resonance depends on the microenvironment and the doublet band thus reports about this. The H unit doublet arises from coupling between the normal mode Q15 (observed at 843 cm^{-1}) and the second harmonic of Q6 the fundamental of which is predicted at 407 cm^{-1} (scaled) or 425 cm^{-1} (anharmonic corrected) but not observed in the Raman spectrum. The ratio of the component intensities strongly depends on the intermolecular hydrogen bonding state of the phenoxy group.⁴⁹ In the present case, $I_{843}/I_{823} = 3.77$ corresponds well to the nonhydrogen bonding CCl_4 solvent.

As for the tyrosine units in proteins, this information can thus in principle be used to obtain information regarding the environment hydrogen bonding state of the phenolic H-units in lignin or DHP. However, in practice, lignin samples are composed of a significantly larger amount of substructural types than those considered in the present work. At the present state of knowledge it is not known to which degree other substructural types respond to the environment, and whether their Raman bands and changes of these can be separated from those of the phenolic H-units. Thus, the vibrational behavior of at least all dominant substructural types would need to be predicted and verified to establish any possible interference. This is not within the range of the present work but sets a goal for future work on the prediction of important features of lignin Raman spectra.

Conclusions

NIR FT-Raman spectra of three models of the H, G, and S types of lignin phenolic end groups have been compared with DFT predictions of their vibrational properties in CCl_4 solvent.

The two methods of correcting harmonic frequencies to better fit fundamentals both have worst performance for the high frequency CH stretch vibrations, with rms errors ~ 40 – 50 cm^{-1} . For the low frequency vibrations a significant better performance is obtained, where ip vibrations are predicted with an overall error of 11 cm^{-1} , using an HF anharmonic frequency shift correction, and 19 cm^{-1} , using a frequency scaling factor. For the oop vibrations there was an overall error of 14 cm^{-1} using the conventional scaling approach and 28 cm^{-1} for the anharmonic frequency shift correction approach. The latter was reduced to 19 cm^{-1} by excluding the CH_3 umbrella vibration at 1379 cm^{-1} .

Thus, for the “fingerprint” region $<1800\text{ cm}^{-1}$ DFT-based methods offer the possibility of qualifying the assignment of Raman bands of lignin and lignin models, thereby helping to avoid incorrect spectral band assignments. The calculation of anharmonic frequency shifts furthermore removes the empirical dependency inherent in the scaling factor approach. Considering that the HF and B3LYP methods and the limited size basis set can introduce errors there is even room for improvements.

For a full assignment of the S unit, the multiple-conformer nature of the non-hydrogen-bonded methoxy group must be considered. Even though the 0° conformer is energetically biased a few vibrations have been identified as intensity (and some frequency) sensitive to the 120° conformer population. PCM calculations show that these vibrations can report on the S unit environment (hydrogen bonding) via the coupling of environment with population probability. By the same mechanism the environment temperature can affect the relative distribution of Raman intensity between the two conformers, the 120° conformer being biased by increasing temperature.

The following marker bands for the three lignin model monomers were found: H units, an intense band at ap-

proximately 840 cm^{-1} ; G units, a doublet of intense bands at 700 and 800 cm^{-1} , a medium intense doublet at 1272 and 1288 cm^{-1} ; S units, a medium to intense doublet at 1452 and 1465 cm^{-1} and an intense band at 1331 cm^{-1} .

The interval from 1700 to 1100 cm^{-1} offers other well-defined bands to be used in identifying the different lignin model monomers. The two ring deformations modes at 1600 cm^{-1} can by polarized spectroscopy inform on lignin structure and ring orientation or can, in addition to a few other vibrational modes, inform on the microenvironment of lignin models.

Acknowledgment. Professor O. F. Nielsen and technician L. Ryelund, Department of Chemistry, University of Copenhagen, are thanked for their assistance in obtaining the Raman spectra. This research was supported by the The Danish Council for Independent Research, Technology and Production Sciences (FTP).

References and Notes

- (1) Sjöström, E. *Wood Chemistry—Fundamentals and Applications*, 2nd ed.; Academic Press, Inc.: San Diego, 1993.
- (2) Whetten, R. W.; MacKay, J. J.; Sederoff, R. R. Recent Advances in Understanding Lignin Biosynthesis. *Annu. Rev. Plant Physiol. Plant Mol. Biol.* **1998**, *49*, 585–609.
- (3) Agarwal, U. P.; Atalla, R. H. Raman Spectral Features Associated with Chromophores in High-Yield Pulps. *J. Wood Chem. Technol.* **1994**, *14*, 227–241.
- (4) Atalla, R. H.; Agarwal, U. P. Recording Raman-Spectra from Plant-Cell Walls. *J. Raman Spectrosc.* **1986**, *17* (2), 229–231.
- (5) Faix, O. Classification of Lignins from Different Botanical Origins by FT-IR Spectroscopy. *Holzforschung* **1991**, *45*, 21–27.
- (6) Atalla, R. H.; Agarwal, U. P.; Bond, J. S. *Methods in Lignin Chemistry*; Springer Verlag: New York, 1992; p 162.
- (7) Agarwal, U. P.; Reiner, S. R. Near-IR Surface Enhanced Raman Spectrum of Lignin. *J. Raman Spectrosc.* **2009**, *40*, 1527–1534.
- (8) Kihara, M.; Takayama, M.; Wariishi, H.; Tanaka, H. Determination of the Carbonyl Groups in Native Lignin Utilizing Fourier Transform Raman Spectroscopy. *Spectrochim. Acta, Part A* **2002**, *58*, 2213–221.
- (9) Agarwal, U. P.; Landucci, L. L. FT-Raman Investigation of Bleaching of Spruce Thermomechanical Pulp. *J. Pulp Pap. Sci.* **2004**, *30*, 269–274.
- (10) Agarwal, U. P.; Ralph, S. A. FT-Raman Spectroscopy of Wood Identifying Contributions of Lignin and Carbohydrate Polymers in the Spectrum of Black Spruce (*Picea mariana*). *Appl. Spectrosc.* **1997**, *51*, 1648–1655.
- (11) Stewart, D.; Yahiaoui, N.; McDougall, G. J.; Myton, K.; Marque, C.; Boudet, A. M.; Haigh, J. Fourier-Transform Infrared and Raman Spectroscopic Evidence for the Incorporation of Cinnamaldehydes into the Lignin of Transgenic Tobacco (*Nicotiana tabacum L.*) Plants with Reduced Expression of Cinnamyl Alcohol Dehydrogenase. *Planta* **1997**, *201*, 311–318.
- (12) Barsberg, S.; Matousek, P.; Towrie, M. Structural Analysis of Lignin by Resonance Raman Spectroscopy. *Macromol. Biosci.* **2005**, *5*, 743–752.
- (13) Barsberg, S.; Matousek, P.; Towrie, M.; Jorgensen, H.; Felby, C. Lignin Radicals in the Plant Cell Wall Probed by Kerr-Gated Resonance Raman Spectroscopy. *Biophys. J.* **2006**, *90*, 2978–2986.
- (14) Jaaskelainen, A. S.; Saariaho, A. M.; Vyorykka, J.; Vuorinen, T.; Matousek, P.; Parker, A. W. Application of UV-Vis and Resonance Raman Spectroscopy To Study Bleaching and Photoyellowing of Thermomechanical Pulps. *Holzforschung* **2006**, *60*, 231–238.
- (15) Larsen, K. L.; Barsberg, S.; Ronayne, K. L.; Parker, A. W.; Matousek, P.; Towrie, M. Kerr-Gated Resonance Raman Spectroscopy in the Studies of Lignin Polymerization. *Annual Report 2004–2005*; Council Cent. Lab. Research Councils: Chilton Didcot, U.K., 2005.
- (16) Saariaho, A. M.; Jaaskelainen, A. S.; Nuopponen, M.; Vuorinen, T. Ultraviolet Resonance Raman Spectroscopy in Lignin Analysis: Determination of Characteristic Vibrations of *p*-Hydroxyphenyl, Guaiacyl, and Syringyl Lignin Structures. *Appl. Spectrosc.* **2003**, *57*, 58–66.
- (17) Saariaho, A. M.; Argyropoulos, D. S.; Jaaskelainen, A. S.; Vuorinen, T. Development of the Partial Least Squares Models for the Interpretation of the UV Resonance Raman Spectra of Lignin Model Compounds. *Vib. Spectrosc.* **2005**, *37*, 111–121.
- (18) Vikkula, A.; Vuorinen, T. The Formation of LC and Other Aromatic End-Group Structures in *O*-Alkyl-Substituted Cellulose during Kraft Pulping Conditions. *J. Wood Sci.* **2007**, *53* (3), 229–233.
- (19) Hohenberg, P.; Kohn, W. Inhomogeneous Electron Gas. *Phys. Rev.* **1964**, *136*, 864.
- (20) Kohn, W.; Sham, L. J. Quantum Density Oscillations in an Inhomogeneous Electron Gas. *Phys. Rev.* **1965**, *137*, 1697.
- (21) Becke, A. D. A New Mixing of Hartree-Fock and Local Density Functional Theories. *J. Chem. Phys.* **1993**, *98*, 1372–1377.
- (22) Lee, C. T.; Yang, W. T.; Parr, R. G. Development of the Colle-Salvetti Correlation-Energy Formula into a Functional of the Electron Density. *Phys. Rev. B* **1988**, *37*, 785–789.
- (23) Stephens, P. J.; Devlin, F. J.; Chabalowski, C. F.; Frisch, M. J. Ab Initio Calculation of Vibrational Absorption and Circular-Dichroism Spectra Using Density Functional Force Fields. *J. Phys. Chem.* **1994**, *98*, 11623–11627.
- (24) Vosko, S. H.; Wilk, L.; Nusair, M. Accurate Spin-Dependent Electron Liquid Correlation Energies for Local Spin-Density Calculations—A Critical Analysis. *Can. J. Phys.* **1980**, *58*, 1200–1211.
- (25) Kärkönen, A.; Koutaniemi, S. Lignin Biosynthesis Studies in Plant Tissue Cultures. *J. Integr. Plant Biol.* **2010**, *52*, 176–185.
- (26) Frisch, M. J.; Trucks, G. W.; Schlegel, H. B.; Scuseria, G. E.; Robb, M. A.; Cheeseman, J. R.; Montgomery, J. A., Jr.; Vreven, T.; Kudin, K. N.; Burant, J. C.; Millam, J. M.; Iyengar, S. S.; Tomasi, J.; Barone, V.; Mennucci, B.; Cossi, M.; Scalmani, G.; Rega, N.; Petersson, G. A.; Nakatsuji, H.; Hada, M.; Ehara, M.; Toyota, K.; Fukuda, R.; Hasegawa, J.; Ishida, M.; Nakajima, T.; Honda, Y.; Kitao, O.; Nakai, H.; Klene, M.; Li, X.; Knox, J. E.; Hratchian, H. P.; Cross, J. B.; Bakken, V.; Adamo, C.; Jaramillo, J.; Gomperts, R.; Stratmann, R. E.; Yazyev, O.; Austin, A. J.; Cammi, R.; Pomelli, C.; Ochterski, J. W.; Ayala, P. Y.; Morokuma, K.; Voth, G. A.; Salvador, P.; Dannenberg, J. J.; Zakrzewski, V. G.; Dapprich, S.; Daniels, A. D.; Strain, M. C.; Farkas, O.; Malick, D. K.; Rabuck, A. D.; Raghavachari, K.; Foresman, J. B.; Ortiz, J. V.; Cui, Q.; Baboul, A. G.; Clifford, S.; Cioslowski, J.; Stefanov, B. B.; Liu, G.; Liashenko, A.; Piskorz, P.; Komaromi, I.; Martin, R. L.; Fox, D. J.; Keith, T.; Al-Laham, M. A.; Peng, C. Y.; Nanayakkara, A.; Challacombe, M.; Gill, P. M. W.; Johnson, B.; Chen, W.; Wong, M. W.; Gonzalez, C.; Pople, J. A. *Gaussian 03*, revision D.01; Gaussian, Inc.: Wallingford, CT, 2004.
- (27) Koury, J. *Guide for Raman Shift Standards for Spectrometer Calibration in Annual Book ASTM Standards*; ASTM: West Conshohocken, PA, 1996; Vol. 0306.
- (28) Mann; C. K. Vickers, T. J. The Quest for Accuracy in Raman Spectra. In *Handbook of Raman Spectroscopy*; Lewis, I. R., Edwards, H. G. M., Eds.; Marcel Dekker, Inc.: New York, 2001; pp 251–274.
- (29) Merrick, J. P.; Moran, D.; Radom, L. An evaluation of harmonic vibrational frequency scale factors. *J. Phys. Chem. A* **2007**, *111*, 11683–11700.
- (30) Agache, C.; Popa, V. I. Ab initio studies on the molecular conformation of lignin model compounds I. Conformational preferences of the phenolic hydroxyl and methoxy groups in guaiacol. *Monatsh. Chem.* **2006**, *137*, 55–68.
- (31) Jalbout, A. F.; Nazari, F.; Turker, L. Gaussian-Based Computations in Molecular Science. *J. Mol. Struct.* **2004**, *671*, 1–21.
- (32) Ditchfield, R.; Hehre, W. J.; Pople, J. A. Self-Consistent Molecular-Orbital Methods 0.9. Extended Gaussian-Type Basis for Molecular-Orbital Studies of Organic Molecules. *J. Chem. Phys.* **1971**, *54*, 724.
- (33) Gordon, M. S. The Isomers of Silacyclop propane. *Chem. Phys. Lett.* **1980**, *76*, 163–168.
- (34) Harihara, P. C.; Pople, J. A. Accuracy of Ah Equilibrium Geometries by Single Determinant Molecular-Orbital Theory. *Mol. Phys.* **1974**, *27*, 209–214.
- (35) Hehre, W. J.; Ditchfield, R.; Pople, J. A. Self-Consistent Molecular-Orbital Methods 0.12. Further Extensions of Gaussian-Type Basis Sets for Use in Molecular-Orbital Studies of Organic Molecules. *J. Chem. Phys.* **1972**, *56*, 2257.
- (36) Helgaker, T.; Klopper, W.; Tew, D. P. Quantitative Quantum Chemistry. *Mol. Phys.* **2008**, *106*, 2107–2143.
- (37) Barsberg, S. Evaluation of Recent Scaling Free Methods to Predict Phenol and Phenoxyl Radical Vibrational Properties—Guidelines for More Complex Models of Lignin or Protein Moieties. *Int. J. Quantum Chem.* **2009**, *109*, 1531–1546.
- (38) Atalla, R. H.; Agarwal, U. P. Raman Microprobe Evidence for Lignin Orientation in the Cell Walls of Native Woody Tissue. *Science* **1985**, *227*, 636–638.
- (39) Pandey, K. K.; Vuorinen, T. UV Resonance Raman Spectroscopic Study of Photodegradation of Hardwood and Softwood Lignins by UV Laser. *Holzforschung* **2008**, *62*, 183–188.
- (40) Kondo, R.; Iimori, T.; Imamura, H.; Nishida, T. Polymerization of Dhp and Depolymerization of Dhp-Glucoside by Lignin Oxidizing Enzymes. *J. Biotechnol.* **1990**, *13*, 181–188.
- (41) Terashima, N.; Atalla, R. H.; Ralph, S. A.; Landucci, L. L.; Lapierre, C.; Monties, B. New Preparations of Lignin Polymer Models under Conditions that Approximate Cell Wall Lignification. II. Structural Characterization of the Models by Thioacidolysis. *Holzforschung* **1996**, *50*, 9–14.
- (42) Lairez, D.; Cathala, B.; Monties, B.; Bedos-Belval, F.; Duran, H.; Gorrichon, L. Aggregation During Coniferyl Alcohol Polymerization in

Pectin Solution: A Biomimetic Approach of the First Steps of Lignification. *Biomacromolecules* **2005**, *6*, 763–774.

(43) Landucci, L. L.; Ralph, S. A.; Hammel, K. E. C-13 NMR Characterization of Guaiacyl, Guaiacyl/Syringyl, and Syringyl Dehydrogenation Polymers. *Holzforschung* **1998**, *52*, 160–170.

(44) Freudenberg, K. Lignin—Its Constitution and Formation from *p*-Hydroxycinnamyl Alcohols. *Science* **1965**, *148*, 595.

(45) Agarwal, U. P. An Overview of Raman Spectroscopy as Applied to Lignocellulosic Materials. In *Advances in Lignocellulosics Characterization*, TAPPI Press: Atlanta, GA, 1999; p 201.

(46) Takahashi, R.; Noguchi, T. Criteria for Determining the Hydrogen-Bond Structures of a Tyrosine Side Chain by Fourier Transform Infrared Spectroscopy: Density Functional Theory Analyses of Model Hydrogen-Bonded Complexes of *p*-Cresol. *J. Phys. Chem. B* **2007**, *111*, 13833–13844.

(47) Takeuchi, H.; Watanabe, N.; Harada, I. Vibrational Spectra and Normal Coordinate Analysis of *p*-Cresol and Its Deuterated Analogs. *Spectrochim. Acta, Part A* **1988**, *44*, 749–761.

(48) Siamwiza, M. N.; Lord, R. C.; Chen, M. C.; Takamatsu, T.; Harada, I.; Matsura, H.; Shimanouchi, T. Interpretation of Doublet at 850 and 830 cm^{-1} in Raman Spectra of Tyrosyl Residues in Proteins and Certain Model Compounds. *Biochemistry* **1975**, *14*, 4870–4876.

(49) Arp, Z.; Autrey, D.; Laane, J.; Overman, S. A.; Thomas, G. J. Structural Studies of Viruses by Raman Spectroscopy Part LXI—Tyrosine Raman Signatures of the Filamentous Virus Ff are Diagnostic of Non-Hydrogen-Bonded Phenoxyls: Demonstration by Raman and Infrared Spectroscopy of *p*-Cresol Vapor. *Biochemistry* **2001**, *40*, 2522–2529.

JP1028239